Science Advances

AAAS

advances.sciencemag.org/cgi/content/full/2/12/e1600452/DC1

Supplementary Materials for

Receptor dimer stabilization by hierarchical plasma membrane microcompartments regulates cytokine signaling

Changjiang You, Tatiana T. Marquez-Lago, Christian Paolo Richter, Stephan Wilmes, Ignacio Moraga, K. Christopher Garcia, André Leier, Jacob Piehler

Published 2 December 2016, *Sci. Adv.* **2**, e1600452 (2016)
DOI: 10.1126/sciadv.1600452

The PDF file includes:

- fig. S11. Dependency of simulated receptor complex lifetime on MSK hop probability.
- fig. S12. Effect of the reaction radius on the simulated receptor complex lifetime.
- fig. S13. TALM and pcTALM analyses of receptor confinement.
- fig. S14. Primary and secondary confinement confirmed by tracking receptors at 2000 Hz.
- fig. S15. Compartment size and dwell time determined by DBSCAN analysis of fast TALM images.
- fig. S16. Spatial stochastic model for simulating hierarchical confinement zones.
- fig. S17. Fitting of hop probabilities in the refined MSK model.
- fig. S18. Experimental trajectory length histograms for different colocalization cutoffs.
- fig. S19. Channel alignment for colocalization analysis.
- fig. S20. Determination of the observation window for time-lapse pcTALM.
- Legends for movies S1 to S7
- References (*69*–*71*)

Other Supplementary Material for this manuscript includes the following:
(available at advances.sciencemag.org/cgi/content/full/2/12/e1600452/DC1)

- movie S1 (.avi format). Controls confirming the labeling specificity.
- movie S2 (.avi format). Dual-color single-molecule imaging of QD-labeled IFNAR1 and IFNAR2 in a live cell.
- movie S3 (.avi format). Characterization of receptor diffusion before and after IFN stimulation.
- movie S4 (.avi format). Assembly and dissociation of ternary complexes revealed by single-molecule tracking.
- movie S5 (.avi format). Diffusion, dissociation, and reassociation of an individual ternary complex in the MSK meshwork, as obtained from spatial simulations.
- movie S6 (.avi format). Experimentally observed receptor rebinding events.
- movie S7 (.avi format). Transient receptor confinement at the native cell PM observed by fast TALM.

section S1. Description of the spatial stochastic models and the simulations

1 Modeling diffusion and interaction in the plasma membrane

1.1 Basic model parameterization

In order to quantitatively investigate the compartmentalization effect induced by the membrane skeleton (MSK), we built a model of receptor binding dynamics and diffusion on a compartmentalized, two-dimensional plasma membrane. The model's physical properties were chosen such that the simulated receptor diffusion closely mimicked live cell observations both in the presence and absence of compartmental barriers. We implemented and simulated the model using *Smoldyn* (*67*), a particle-based spatial-stochastic simulator. The basic model of an uncompartmentalized homogeneous membrane required specification of certain key parameters such as the size of the two-dimensional model membrane (i.e. the domain), the diffusing species, their diffusion constants, association and dissociation rates, and the time step of the simulator. The latter determines the spatial resolution of the simulation.

The membrane was defined as a squared area of size 10×10 μm^2 with reflecting boundary conditions. Compared to experimentally observed MSK compartment sizes with an average diameter of less than 200 nm (*3*, *6*, *42*) our model domain size was more than 10^3 times larger. Thus, our domain was large enough such that statistics of binding dynamics and diffusive behavior were sampled over a large number of compartments, guaranteeing statistical significance of our assessment of the compartmentalization effect. Moreover, given our total simulation time is in the order of seconds, boundary effects could be safely ignored for particle trajectories starting near the domain center.

The diffusing species in the model membrane were R1 (IFNAR1), R2 (the binary complex of IFNAR2/IFNα2), and T (the ternary complex of IFNAR1/IFNAR2/IFNα2). Here, the binding of IFNα2 from solution did not require explicit modeling, as the stability of the binary complex of IFNAR2/IFNα2 is far beyond the time scale of our model. Specifically, a half-life of ~50 s for the IFNAR2/IFNα2 binary complex was measured (*34*). This is three orders of magnitude higher than the trapping time of receptors in MSK compartments as previously reported (*3*).

The associated diffusion constant of each modeled species was specified by the corresponding microdiffusion constant D_{micro}, that is, the molecule's free diffusion constant. A microdiffusion constant for R1 and R2 of

$D_{\mathrm{R1/R2}} = 1.1$ µm²/s was experimentally obtained by single molecule tracking of diffusing IFNAR1 and IFNAR2 on polymer-supported membranes (*43*, *44*). Aside, the diffusion constant of the ternary complex T was measured as $D_{\mathrm{T}} = 0.7$ µm²/s (*43*) which is close to the value predicted by the Saffman–Delbrück formula (*69*).

According to the theoretical framework of *Smoldyn*, a model's spatial resolution s is defined as the average displacement of a molecule of the fastest diffusing species. Hence, to achieve a certain spatial resolution s the simulation time step needs to obey

$$\Delta t < \frac{s^2}{2D_{\mathrm{max}}} \qquad \text{(Eqn. S1)}$$

where D_{max} is the largest diffusion coefficient of all species in the model (cf. *Smoldyn* User Manual). For our model, the largest diffusion coefficient was given by the microdiffusion constant of R1 and R2. Hence, for $D_{\mathrm{R1/R2}} = 1.1$ µm²/s and $\Delta t = 0.005$ ms we achieved a spatial resolution of 4.7 nm.

For the purpose of model validation we performed simulations with different values of $D_{\mathrm{R1/R2}}$. However, the spatial resolution had to be identical for all scenarios in order to guarantee comparability of our simulation results. This was achieved by modifying the simulation time steps according to eqn. S1. Table S2 lists the corresponding Δt for different values of $D_{\mathrm{R1/R2}}$.

Receptor association was fully characterized in terms of two parameters, the association radius r_{on} and the probability of binding p_{on}. The first parameter (r_{on}) was identified with the cross section distance for two receptors undergoing a collision, which has a value of approximately 5-10 nm, as previously determined by cryo-EM (*70*). Thus, our choice of Δt also guaranteed that the model's spatial resolution was smaller than r_{on}. The parameter p_{on}, which defines the probability of a productive collision, was fitted against experimental data. For that purpose, we closely mimicked the corresponding experimental conditions by simulating free diffusion and irreversible association of 5000 IFNAR1 and 100 IFNAR2 molecules in the uncompartmentalized membrane with reflective boundary conditions. Figure S9a shows the perfect match between the simulated and the experimentally observed irreversible association dynamics when adopting parameter values $D_{\mathrm{R1/R2}} = 1.1$ µm²/s, $\Delta t = 0.005$ ms, $r_{\mathrm{on}} = 5$ nm, and $p_{\mathrm{on}} = 0.0068$. Obviously, any changes to $D_{\mathrm{R1/R2}}$, Δt, and r_{on} require re-fitting, yielding a different binding probability p_{on}. table S2 shows additional fitting results of p_{on} for different diffusion constants and time-steps. Figure S9b shows the irreversible association curve for $r_{\mathrm{on}} = 10$ nm and $p_{\mathrm{on}} = 0.0017$ ($D_{\mathrm{R1/R2}} = 1.1$ µm²/s, $\Delta t = 0.005$ ms) perfectly matching the experimental data. For receptor dissociation, a reaction rate k_{off}

was set to an experimentally derived value of 0.3 s^{-1}. For details on how association and dissociation events are simulated we refer to the *Smoldyn* User Manual and reference (*67*).

1.2 Modeling the MSK mesh

In a thorough study of MSK compartment sizes (*3*) diameter ranges of 32-110 nm were reported for various human cells. However, our experiments were performed on U5A cells, a human lung fibrosarcoma cell line where cells lack IFNAR2 but express IFNAR1. For such cells, no MSK compartment size has been reported so far. Therefore, we decided to use as a reference value 68 nm which is the median of MSK compartment sizes measured from HeLa cells, the most commonly used human cancer cell line.

MSK compartmentalization was introduced to the model in form of a triangular mesh (fig. S7) that was created by using distmesh2d (*3*), up to and including the very first re-triangulation step. More specifically, a Delaunay triangulation was performed on a union of two point sets, namely a set of randomly distributed points in the inner area of the modeled 10×10 μm^2 domain (0.1 µm away from the boundary) and a set of fixed points placed on each edge, with a 70 nm distance between each other. Acceptance of points for subsequent triangulation was based on a scaled edge length function (*3*). This, in turn, was defined as a gamma function that was fitted to a scaled distribution of compartment sizes of FRSK cells as previously reported (*3*, *6*). Scaling of this distribution by a factor of 1.7 was necessary to account for the differences in cell types, as FRSK cells have a reported median MSK compartment size of 41 nm while the one for HeLa cells is about 68 nm. From a series of randomly generated domain triangulations, we selected one that had a median of ~70 nm, which was closest to our reference value of 68 nm.

The resulting triangular compartments were imported into *Smoldyn* by defining a surface object (cf. *Smoldyn* terminology) consisting of the unique set of all triangle sides, each of which was specified as a 2D panel (cf. *Smoldyn* terminology). This allowed us to define individual hop probabilities for each species (R1, R2, and T) and uniformly for all triangle boundaries and for both hop directions across triangle sides (cf. Section “Hop diffusion in the MSK model”).

Moreover, we also defined for each compartment a corresponding *Smoldyn* surface with an associated binding reaction to ensure that binding between R1 and R2 occurred only when both receptors resided in the same compartment (and not among non-colocalized binding partners). All binding reactions were set to be identical,

i.e., to have the same r_{on} and p_{on} as the association reaction previously defined for the uncompartmentalized domain, but now defined to be compartment-specific. Dissociation of the ternary complex was not defined to be compartment-specific and, hence, introducing the MSK did not require any changes with respect to the dissociation reaction. However, the location of the dissociated product molecules was specified to be the position of the former complex with zero offset. This was necessary to guarantee that product molecules were placed into the same compartment as the former complex, especially so when dissociation occurred close to a compartment boundary.

1.3 Hop diffusion in the MSK model

Using $D_{R1/R2} = 1.1$ μm²/s and $\Delta t = 0.005$ ms, we manually fitted the MSK hop probability for both IFNAR1 and IFNAR2 (p_{MSK}). This was accomplished by comparing 160 ms jump length statistics (molecule displacements at 160 ms intervals) acquired from simulations for various p_{MSK} values with the experimentally obtained distributions for IFNAR1 and IFNAR2 (cf. Section "Colocalization analysis and single particle tracking"). Such experimental jump length distributions were obtained from wt cells. Distributions of displacements were obtained by simulating the diffusion of 200 receptors (without reactions) in the MSK-compartmentalized domain. Individual particle positions were recorded every 160 ms. At $t = 0$, all molecules were given an initial random position inside the 4×4 μm² crop around the center of the domain. The latter was done to avoid any side effects of the domain's boundary. By varying p_{MSK} in steps of 0.00005, we obtained the best fit with $p_{MSK} = 0.00095$ (fig. S8a). Similarly, we fitted MSK hop probabilities with experimental jump length distributions obtained from LatB-treated cells. For $D_{R1/R2} = 1.1$ μm²/s and $\Delta t = 0.005$ ms and by varying p_{MSK} in steps of 0.0002, we achieved a good fit with $p_{MSK} = 0.0036$ (fig. S8b). We also fitted the MSK hop probability p_{MSK} for $D_{R1/R2} = 5$ μm²/s and $\Delta t = 0.0011$ ms against the experimental wt jump length distribution and obtained a good match with $p_{MSK} = 0.0002$ (fig. S8c). The reduced value for p_{MSK} was expected since the almost 5-fold larger diffusion constant inevitably creates more interaction events between the particle and compartment boundaries per unit of time.

Lastly, we also fitted MSK hop probabilities for ternary complexes T with experimentally derived jump length distributions. When assuming $D_T = 0.7$ μm²/s and $\Delta t = 0.005$ ms, a good fit was obtained with $p_{MSK} = 0.0005$. However, studying complex stability and lifetime does not demand a detailed modeling of hop diffusion of T. By consequence, we simply set the hop probability of T to a slightly smaller value than the hop probability fitted for R1/R2, except where explicitly stated.

2. Simulation of receptor dynamics in the MSK model

2.1 Measure of ternary complex lifetime

To study the stability and effective lifetime of ternary complexes, i.e., the time until IFNAR1 and IFNAR2 can no longer be considered colocalized, we simulated receptor association-dissociation dynamics in the MSK-compartmentalized membrane. The simulations were initialized with a single ternary complex, thus avoiding cross-bindings between R1 and R2 molecules of two or more complexes. This ensured that our simulated lifetime results would only exhibit effects caused by "passive confinement".

In order to compare our simulation results with experimental observations, we defined a criterion for R1/R2 colocalization, and hence for the lifetime of the ternary complex, that adequately reflects the experimental localization precision. Three such criteria were assessed for their compatibility with experimental specifications, each of which corresponds to one of the following "non-colocalization" events:

I) R1 and R2 are localized in different MSK triangles.
II) R1 and R2 are separated by at least 150 nm.
III) R1 and R2 are localized in different, non-neighboring MSK triangles.

A measure for the lifetime of a ternary complex is associated with each criterion. This is defined as the period until the corresponding event is observed for the first time.

Our choice of a criterion was based on several considerations. The localization precision of a single QD is on average 20 nm, but in the worst case only ~35 nm. Full separation of R1 and R2 is experimentally detectable only for distances above a threshold of 120 nm (this includes a separation of 15 nm due to the two channel alignment precision). Since the median length scale of MSK compartments is expected to be around 70 nm, any separation of R1 and R2 in the same MSK compartment would likely not be detected experimentally.

Criterion II is MSK-independent as it considers only the distance between R1 and R2, without taking compartmental colocalization into account. In principle, this criterion can be satisfied by receptors inside a single (obtuse-angled) MSK triangle. However, such geometry is rather unlikely and imposing such threshold would potentially bias our analysis. Moreover, a non-colocalization criterion that is not based on the MSK is also less suitable for assessing compartmentalization effects. Therefore, criterion II serves here only as a control measure.

In contrast, criteria I and III support, by definition, the MSK-based separation of R1 and R2. Lifetimes will usually be the shortest if measured according to criterion I, as MSK triangles have a length scale that is shorter than the 150 nm threshold of criterion II. Most importantly, the median length scale of MSK triangles is also considerably shorter than the experimental detection threshold (~120 nm). As a consequence, using criterion I would likely result in a bias towards shorter simulated lifetimes as compared to experimentally measured lifetimes. On the other hand, non-neighboring triangles, i.e. those that do not have a corner point in common, are by default further apart than neighboring triangles. Hence, when one receptor enters a compartment that is not neighboring the compartment of the other receptor, the distance between these two will be closer to the experimental detection threshold. For these reasons, criterion III is expected to yield the most adequate lifetime results and was therefore employed throughout our simulation study of ternary complex lifetimes.

For such simulations the receptor complex was randomly placed within the 4×4 μm^2 area in the center of the model membrane. Positions of R1/R2 or T were recorded every 0.032 s, in correspondence to the conventional frame rate used in single molecule imaging experiments. The total simulation time was set to 15 s. As part of our study, we varied different model parameters (see below) to quantitatively assess how MSK-based compartmentalization affects receptor complex lifetime. For each parameter scenario, we performed 200 simulations and analyzed the recorded receptor positions

In the following sections, the state in which R1 and R2 are either bound or colocalized according to the employed criterion is denoted by T*. The time evolution of the probability of observing T*, $p_{\mathrm{T}*}(t)$, is referred to as colocalization probability dynamics. In turn, the probability of observing T* after 15 s is denoted with $p_{\mathrm{T}*@15\mathrm{s}}$.

The average lifetime is then obtained as $\tau = 1/\lambda$, by fitting $p_{\mathrm{T}*}(t)$ with an exponential function $\exp(-\lambda t)$. Here, it is worth noting if $p_1/p_2 = r$ for two observation probabilities $p_1 = \exp(-\lambda_1 t)$ and $p_2 = \exp(-\lambda_2 t)$ at a given time t, then $\tau_1/\tau_2 = (\log r + \log p_1)/\log p_1$. This relationship shows how differences in the probability of observing T* relate to changes in the corresponding mean lifetime.

Figure S1 shows how lifetimes depend on the choice of the non-colocalization criterion, as could be expected. Specifically, in fig. S1a-c we present average colocalization probability dynamics over 15 s, measured according to the three criteria, using identical parameter values $D_{\mathrm{R1/R2}} = 1.1$ μm^2/s, $p_{\mathrm{on}} = 0.0068$, and $r_{\mathrm{on}} = 5$ nm. Different colors indicate different values of p_{MSK}. Figure S1d shows $p_{\mathrm{T}*@15\mathrm{s}}$ for such p_{MSK} values. Evidently,

lifetimes according to criterion II are significantly shorter than those for criterion III for small hop probabilities, and approach the lifetimes of criterion III with increasing p_{MSK} values. Lifetimes measured according to criterion I are shorter than those measured according to criterion III for hop probabilities below ~0.0002, and longer for larger p_{MSK} values.

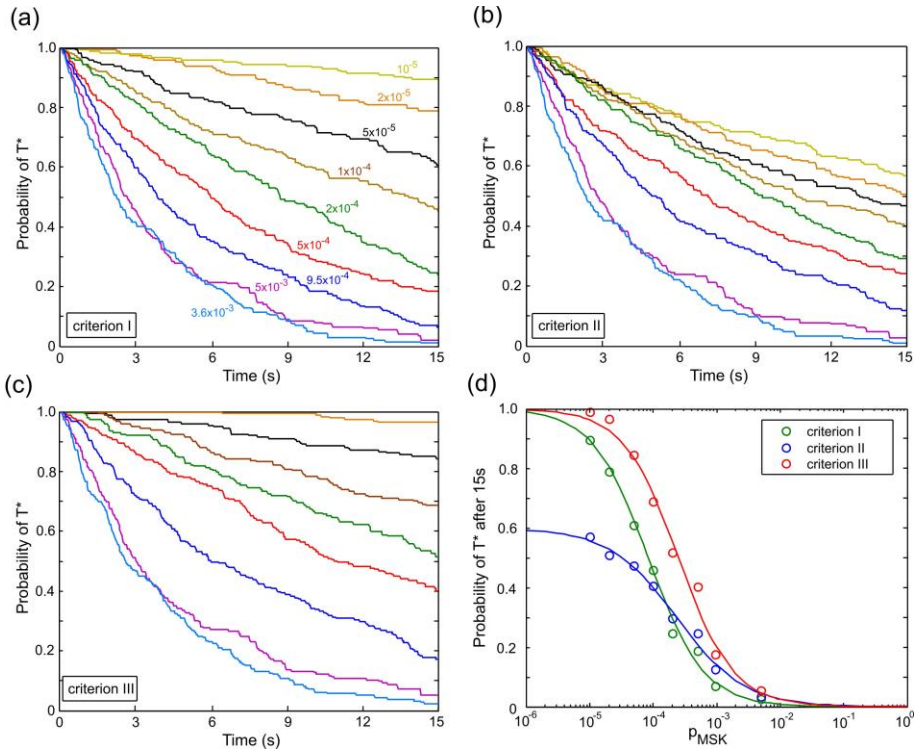

fig. S1. Comparison of non-colocalization criteria. (a-c) Average colocalization probability dynamics over 15 s measured according to the proposed three criteria. Different colors represent different values of p_{MSK} as indicated in (a). Color codes are identical for all three subfigures. In addition, the blue solid and the blue dotted lines correspond to the fitted hop probabilities in the absence and presence of LatB. (d) Probability of observing T* after 15 s ($p_{\mathrm{T*@15s}}$) for all three criteria and for varying values of p_{MSK}. The resulting point plots have been fitted (solid lines) with negative sigmoidal functions, with $f(p_{\mathrm{MSK}}) = 1/\left(1 + (a\, p_{\mathrm{MSK}})^b\right)$ for criterion I and III and with $f(p_{\mathrm{MSK}}) = c/\left(1 + (a\, p_{\mathrm{MSK}})^b\right)$ for criterion II. The fitted parameter values are: a=1.188e4, b=1 (criterion I), a=0.4276e4, b=0.8215, c=0.5993 (criterion II), and a=0.3993e4, b=1.007 (criterion III).

2.2 Simulation of ternary complex lifetimes

The experimentally obtained receptor diffusion constants ($D_{\mathrm{R1/R2}}$, D_{T}) and the fitted kinetic parameters of receptor association and dissociation on the lipid bilayer (p_{on}, r_{on}, k_{off}) were used for our initial simulation study of ternary

complex lifetimes. We will refer to this set of parameter values ($D_{\mathrm{R1/R2}} = 1.1$ µm²/s, $r_{\mathrm{on}} = 5$ nm, $p_{\mathrm{on}} = 0.0068$) as **scenario 1** (cf. table S3).

By using the previously fitted hop probability $p_{\mathrm{MSK}} = 0.00095$ representing hop diffusion in a native cell, we obtained a mean lifetime of 9.4 s (fig. S1c, blue line), which is about 60% of the corresponding experimental value of 15.2 ± 1.7 s. This result highlights the consequences of MSK compartmentalization. For $p_{\mathrm{MSK}} = 0.0036$ (**scenario 1***), representing LatB treated cells, our simulations yielded a mean lifetime of 4.1 s (fig. S1c, light blue line). This is fairly close to the experimentally obtained 4.6 s and the ternary complex lifetime of ~3 s measured on artificial lipid bilayers.

As already mentioned in our discussion of (non-) colocalization criteria above, we performed additional simulations for various hop probabilities in the interval $[10^{-5}, 10^{-2}]$ to obtain a more complete picture of p_{MSK}-dependent ternary complex lifetimes. Figure S1d shows the resulting probabilities $p_{\mathrm{T*@15s}}$ as well as a fit with a negative sigmoidal function, revealing a region of p_{MSK} values where ternary complex lifetimes depend most sensitively on the hop probability.

In order to assess the influence of individual parameter values on our simulation results, we performed additional simulation studies, where we varied either the diffusion constant $D_{\mathrm{R1/R2}}$ (**scenario 1 versus 2**), the reaction radius r_{on} (**scenario 1 versus 3** for different p_{on}, and **scenario 3 versus 4** for similar p_{on}), or the binding probability p_{on} (**scenario 1 versus 4 and 5**). The associated parameters are specified in table S3.

By adopting the parameter set of **scenario 2** ($D_{\mathrm{R1/R2}} = 5$ µm²/s, $\Delta t = 0.0011$ ms, $r_{\mathrm{on}} = 5$ nm, and $p_{\mathrm{on}} = 0.0015$), we investigated the effect of a larger diffusion constant $D_{\mathrm{R1/R2}}$ on the simulated receptor complex lifetime. This choice was deemed valid, given the diffusion constant $D_{\mathrm{R1/R2}}$ is within the previously reported range of 1 to 10 µm²/s. Here, D_{T} was fixed at 3.5 µm²/s in order to preserve the ratio of D_{T} to $D_{\mathrm{R1/R2}}$ from previous simulation studies.

As reported in the Section “Hop diffusion in the MSK model”, the hop probability $p_{\mathrm{MSK}} = 0.0002$ was found to best fit the experimental data for such value of $D_{\mathrm{R1/R2}}$. For this hop probability, the mean lifetime is about $\tau = 10$ s, which is similar to the one in **scenario 1** with fit $p_{\mathrm{MSK}} = 0.00095$ (fig. S11). This result suggests that the

simulated ternary complex lifetime is rather insensitive to changes in the diffusion constant, provided a correct fit of hop probabilities p_{MSK} is considered. In other words, a change in the diffusion constant requires a different p_{MSK} to fit the same jump length distribution, and this compensates for $D_{\mathrm{R1/R2}}$-dependent changes in the colocalization dynamics.

For this parameter scenario, additional simulations with varying hop probabilities p_{MSK} were performed. Figure S11 shows the resulting probabilities of observing T* after 15 s ($p_{\mathrm{T*@15s}}$). In a nutshell, the five times larger $D_{\mathrm{R1/R2}}$ yields a trajectory that is laterally shifted towards smaller values of p_{MSK}, as compared to the corresponding trajectory of **scenario 1**. However, it does not significantly alter the width of the p_{MSK} sensitive region.

To check if the lifetimes are influenced by the choice of reaction radius, we further ran lifetime simulations for parameter **scenario 3** ($D_{\mathrm{R1/R2}} = 1.1$ µm^2/s, $\Delta t = 0.005$ ms, $r_{\mathrm{on}} = 10$ nm, $p_{\mathrm{on}} = 0.0017$, and $p_{\mathrm{MSK}} = 0.00095$). fig. S12 shows a comparison with previous results for $r_{\mathrm{on}} = 5$ nm and $p_{\mathrm{on}} = 0.0068$ of **scenario 1,** which has the same association rate constant as **scenario 3** (fig. S9). The difference after 15 s is negligible (about 3.5% for $p_{\mathrm{T*@15s}}$) which can be attributed to the stochastic nature of our simulations. Thus, in the case that r_{on} and p_{on} are adjusted to yield the same association rate constant, our simulations yielded similar lifetime results for biologically reasonable reaction radii in the range of 5-10 nm, thus validating the stabilizing effect of MSK compartmentalization.

With parameter **scenarios 4 and 5 (**$D_{\mathrm{R1/R2}} = 1.1$ µm^2/s, $\Delta t = 0.005$ ms, $r_{\mathrm{on}} = 5$ nm, $p_{\mathrm{on}} = 0.0018$ and 0.018, respectively), we investigated how the on-rate of receptor association affects the lifetime of the ternary complex. **S**imulation results, $p_{\mathrm{T*@15s}}$ and lifetime τ, for various hop probabilities p_{MSK} are shown in fig. S2, alongside results for $p_{\mathrm{on}} = 0.0068$ (**scenario 1**). Figure S2a ($p_{\mathrm{T*@15s}}$ vs p_{MSK}) reveals regions where the lifetime of the ternary complex depends most sensitively on the hop probability. These regions depend on p_{on} and shift towards larger values with increased binding probability.

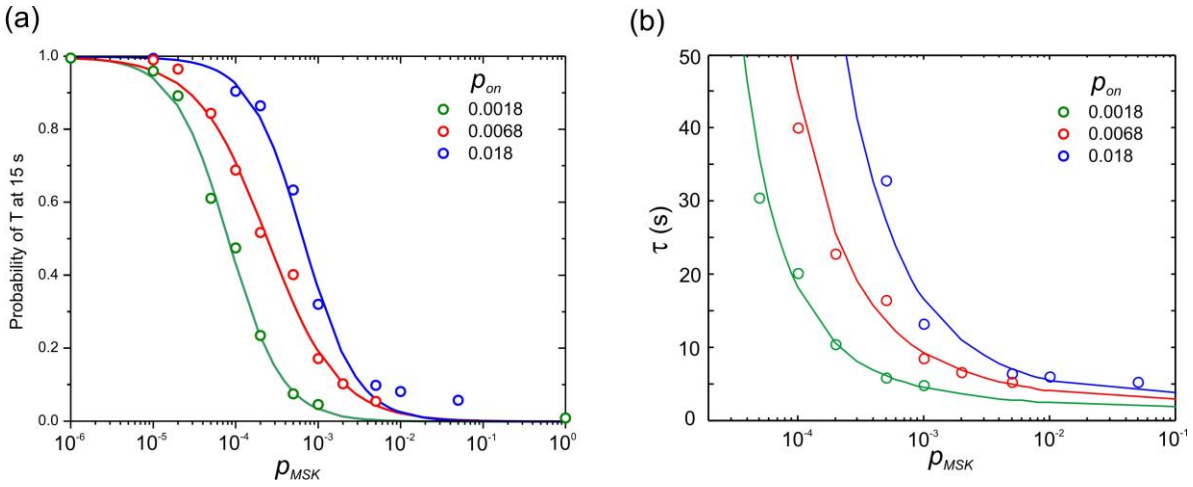

fig. S2. Effect of the binding probability on the simulated receptor complex lifetime. (**a**) Comparison of $p_{\mathrm{T*@15s}}$ *vs* p_{MSK} plots for three different association probabilities p_{on}. Fitted negative sigmoidal curves $f(p_{\mathrm{MSK}}) = 1/\left(1 + (a\, p_{\mathrm{MSK}})^{b}\right)$ are shown as solid lines. The fitting parameters in the case of $p_{\mathrm{on}} = 0.0018$ and $p_{\mathrm{on}} = 0.018$ are: a=1.204e4 and b=1.318 (blue), a=0.1463e4 and b=1.007 (green), a=0.3993e4 and b=1.007 (red), respectively. (**b**) Lifetime trajectories have been calculated from the probabilities and corresponding fitting curves in (a) as $\tau = -t_{\mathrm{end}}/\log p_{\mathrm{T*@15s}}$.

For $p_{\mathrm{on}} = 0.0068$, MSK hopping probabilities close to the previously fitted value of $p_{\mathrm{MSK}} = 0.00095$ start to exert a noticeable effect on the lifetime of ternary complexes. For instance, the probability of observing the ternary complex after 15 s is around 20% for $p_{\mathrm{MSK}} = 0.001$ (according to the fit with a negative sigmoidal curve). The corresponding expected lifetime is ~9.3 s (see the fit in fig. S2b). For a nearly 3.8-fold decreased binding probability (**scenario 4**) such an MSK-based stabilization effect could no longer be observed. Here, the probability, as obtained from the fit, drops below 4% and the corresponding expected ternary complex lifetime is ~4.5 s. On the other hand, an almost two times higher colocalization probability was observed for a ~2.6-fold higher association probability (**scenario 5),** corresponding to a more than 1.5 times larger mean lifetime.

Altogether, our simulations indicate that MSK-induced ternary complex stabilization strongly depends on the association constant. In contrast, for a given association rate constant, we found that the simulated lifetime was rather insensitive to the changes of $D_{\mathrm{R1/R2}}$, and r_{on} (cf. **table S3** for different simulation scenarios).

3 Simulation of ternary complex lifetime in the hierarchical plasma membrane

3.1 Refined membrane model with MSK and secondary compartmentalization

Our experimental results suggest that further organizing principles of the plasma membrane may contribute to ternary complex stabilization. Thus, we extended our membrane model by adding a second level of microcompartmentation.

There are several ways to introduce such a secondary compartmentalization to our membrane model. We opted for a higher-level discretization of the domain with compartment boundaries overlapping those of the MSK (fig. S16a). This was deemed appropriate given the pivotal role of the MSK on the plasma membrane compartmentalization (*13*, *71*) and that our scheme of choice had been previously suggested for hop diffusion of phospholipids (*42*).

To generate the secondary compartmentalization, we employed the following growth algorithm: In the initial step, a pre-specified number of MSK triangles are randomly selected. These triangles become the centers of our secondary compartments (SCs). All SCs grow with the same speed, i.e., each SC undergoes only one growth-step per iteration. In such a step, each SC adds all neighboring MSK triangles (those that share a corner point with the SC) to its existing compartment area, and only triangles that have not already been assigned can be added to a SC. The growth step is repeated until each MSK triangle has been assigned to an SC. Figure S16b illustrates the first two growth steps starting from a center triangle marked with '0'. The borders of the updated SC after the first and second growth step are marked with red and yellow solid lines while all newly added triangles are marked with '1' and '2', respectively.

This method can lead to compartments with areas that are only loosely connected via a single corner point to the rest of the SC. Therefore, we ran a correction algorithm that reduced the number of such distorted compartments by reassigning single, loosely connected triangles to neighboring SCs. Also, since the initial triangles are randomly chosen, the resulting SCs can largely vary in area, shape, and average number of MSKs. Thus, we hand-tuned the number of initial triangles, and re-ran the growth process until the resulting SC length scale (root of SC area) distribution had a mean of around 280nm, corresponding to the experimental value obtained from our cluster analysis (cf. Section "Fast TALM imaging and cluster analysis"). Figure S16b shows our model's SCs in the $4\times4\mu m^2$ crop around the center of the domain while fig. S16c and d show histograms of SC length scales and the number of MSK triangles per SC, respectively.

3.2 Fitting hop probabilities in the refined model

For the two-tiered compartmentalization model, one can either fit p_{SC} while using the previously determined value for p_{MSK}, or allow both jump probabilities p_{MSK} and p_{SC} to be fitted independently. Since the results of LatB treatment (fig. S13) and fast tracking (fig. S14) had pointed out that the secondary compartmentalization is based on the intact membrane skeleton, we introduced a secondary compartmentalization to our MSK model and fitted p_{SC} using the previously determined p_{MSK}. In order to obtain the best fitting, in a first step, we compared the simulation results with the experimentally derived 160 ms-jump length distributions. For a more stringent comparison, fitted hop probabilities were further compared to the calculated R1/R2 median dwell times (DT) of MSK and SC compartments. However, matching the JLD had priority over matching the DTs.

Simulations with $p_{MSK} = p_{SC}$ =0.00095, i.e., without an effective secondary compartmentalization, had yielded median dwell times of 0.11 s (SC) and 40 ms (MSK). In comparison, the experimentally obtained values are 0.43 s for SC (fig. S15) and 28 ms for MSK calculated by $\frac{L^2}{4D_{MACRO}}$where *L*=70nm, *D*=0.043 μm^2/s (table S1). This suggested that, by introducing a secondary compartmentalization to our MSK model, we should obtain a longer dwell time in secondary compartments to mimic the dynamics occurring in living cells. For a fixed MSK hop probability of p_{MSK}=0.00095, the best fits of JLDs and DTs were achieved for p_{SC} =0.00025 by reducing p_{SC} in steps of 0.0001 starting from 0.00095 (fig. S17a). The fitted values yielded median SC and MSK dwell times of 0.49 s and 49 ms, respectively. While the median MSK dwell time was slightly worse as compared to the MSK-only compartmentalization, the SC dwell time was very close to the experimental data.

In a control simulation, by fitting p_{MSK} and p_{SC} independently, we obtained good fits of JLDs for p_{MSK}=0.0015 and p_{SC}=0.0005 (fig. S17b). The obtained median dwell times of 0.25 s for SC and 31 ms for MSK compartments, however, did not show increased ternary complex lifetime. The obtained p_{MSK} of 0.0015 is larger than the intact p_{MSK} of 0.00095, and the dwell time of 0.25 s is much shorter than the experimentally obtained 0.43 s. Both indicate a weaker compartmentalization effect. These results highlight that the compartmentalization effects are heavily dependent on the intact MSK.

3.3 Simulation of ternary complex lifetime in the hierarchical plasma membrane

Using the fitted hop probability of $p_{SC} = 0.00025$ and p_{MSK}=0.00095, we simulated ternary complex dynamics in the model membrane with MSK and secondary compartmentalization. As can be seen from fig. S3, introducing the secondary compartmentalization with fitted hop probability further increases the colocalization probability. The probability of observing T* at t=15 s amounts to 80% of the experimentally derived value. The lifetime obtained from the fit is 12.1 s.

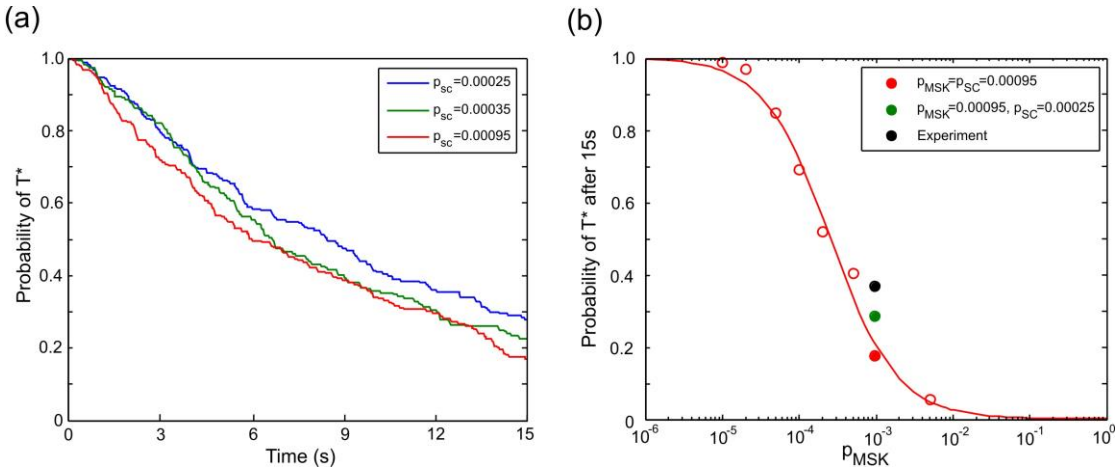

fig. S3. Simulation of ternary complex lifetime in the hierarchical plasma membrane model. (**a**) Time evolution of the probability of observing T* according to criterion III for the two-tiered compartmentalization model with hop probabilities $p_{\mathrm{MSK}} = 0.00095$ and p_{SC} values, as indicated in the legend ($D_{\mathrm{R1/R2}} = 1.1\mu\mathrm{m}^2/\mathrm{s}$, $\Delta t = 0.005\mathrm{ms}$, $r_{\mathrm{on}} = 5\mathrm{nm}$, and $p_{\mathrm{on}} = 0.0068$). (**b**) $p_{\mathrm{T*@15s}}$ *vs* p_{MSK} plots: The red filled circle marks $p_{\mathrm{T*@15s}}$ for the MSK-only scenario, i.e., for hop probabilities $p_{\mathrm{MSK}} = p_{\mathrm{SC}} = 0.00095$; the green dot shows the value of $p_{\mathrm{T*@15s}}$ for the two-tiered compartmentalization with hop probabilities $p_{\mathrm{MSK}} = 0.00095$ and $p_{\mathrm{SC}} = 0.00025$; the black dot marks the experimentally observed lifetime.

table S1. Measured IFN receptor diffusion constants under different conditions. Diffusion constants D_{160ms} and D_{960ms} obtained from squared displacement analyses with lag times of 160 ms and 960 ms, respectively and the fraction *F* of fast and slow components in percent. The data was obtained from ***N*** individual displacements. Averaged values (shown in blue) were calculated by weighting with the fractions of two components.

Species	**D_{160ms} ($\mu m^2/s$)**	***F* (%)**	**D_{960ms} ($\mu m^2/s$)**	***F* (%)**	**D_{160ms}/D_{960ms}**	***N***
IFNAR1	0.051± 0.001	84.7	0.0502± 0.0005	82.4	1.07	9637 /3614
	0.016± 0.001	15.2	0.0085± 0.0004	17.6		
	0.046± 0.003		0.043± 0.002			
IFNAR2	0.050± 0.001	84.2	0.0455± 0.0006	87.0	1.09	9318 /3416
	0.016± 0.001	15.8	0.0104± 0.0008	13.0		
	0.045± 0.003		0.041± 0.003			
IFNAR1 (+IFN)	0.052± 0.001	74.3	0.0373± 0.0007	81.3	1.30	10808 /4902
	0.016± 0.001	25.7	0.0050± 0.0004	18.7		
	0.043± 0.001		0.031± 0.003			
IFNAR2 (+IFN)	0.051± 0.001	73.1	0.0374± 0.0008	83.5	1.27	10969 /4164
	0.016± 0.001	27.9	0.0085± 0.0008	16.5		
	0.042± 0.002		0.033± 0.003			
IFNAR1-IFNAR2 (+IFN)	0.032± 0.001	60.2				1492
	0.0075± 0.0002	39.8				
	0.022± 0.001					
IFNAR1 (+IFN +LatB)	0.082± 0.001	79.7	0.0678± 0.0008	93.9	1.06	35107 /17818
	0.016± 0.001	20.3	0.0026± 0.0006	6.1		
	0.068± 0.004		0.064± 0.004			
IFNAR2 (+IFN +LatB)	0.074± 0.001	82.4	0.0648± 0.0009	95.2	1.03	34532 /14891
	0.016± 0.001	17.6	0.0026± 0.0009	4.8		
	0.064± 0.005		0.062± 0.004			
IFNAR1-IFNAR2 (+IFN +LatB)	0.074± 0.001	66.3				1197
	0.0106± 0.0004	33.7				

table S2. Calculated binding probability p_{on} for different microscopic diffusion constant D_{micro}. Simulation time steps Δt required at different microscopic diffusion constants D_{micro} to achieve the same spatial resolution $s = 4.7$ nm and association probabilities p_{on} calculated to reproduce the experimentally observed in vitro association kinetics.

D_{micro}	Δt	p_{on}
1.1	5e-6	0.0068
1.3	4.23e-6	0.0058
5	1.1e-6	0.0015
9.5	5.79e-7	0.0008

table S3. Parameter scenarios ($D_{R1/R2}$, Δt, r_{on}, and p_{on}) and mean lifetimes τ for fitting hop probabilities.

Scenario	$D_{R1/R2}$ (μm²/s)	Δt (ms)	r_{on} (nm)	p_{on}	p_{MSK}	τ (s)
1	1.1	0.005	5	0.0068	0.00095	9.4
1*	1.1	0.005	5	0.0068	0.0036	4.1
2	5	0.0011	5	0.0015	0.0002	10
3	1.1	0.005	10	0.0017	0.00095	8.2
4	1.1	0.005	5	0.0018	0.00095	5.5
5	1.1	0.005	5	0.018	0.00095	14.8

table S4. Experimental properties of primary and SCs obtained at different time resolution. D_{MACRO}, long-term diffusion constant according to Eqn. 7; D_{micro}, short-term diffusion constant according to Eqn. 7. Note that D_{micro} at 32 ms time lapse corresponds to D_{MACRO} at 0.5 ms time lapse; L, compartment diameter according to Eqn. 7; τ_{comp}, residence time within the compartment according to Eqn. 8; $\tau_{barrier}$, time for the molecule to experience the effect of the barrier of the confinement according to Eqn. 9.

Temporal resolution	**0.5 ms**		**32ms**	
Cell state	**native**	**LatB-treated**	**native**	**LatB-treated**
D_{MACRO} **(μm²/s)**	0.051±0. 011	0.10±0. 01	0.005±0. 002	0.032±0. 037
D_{micro} **(μm²/s)**	0.29±0.19	0.25±0.04	0.050±0.024	0.10±0.02
L **(nm)**	85±11	168±9	304±30	799±398
τ_{comp}	35 ms	72 ms	4.5 s	5.0 s
$\tau_{barrier}$	6.2 ms	28 ms	0.45 s	1.6 s

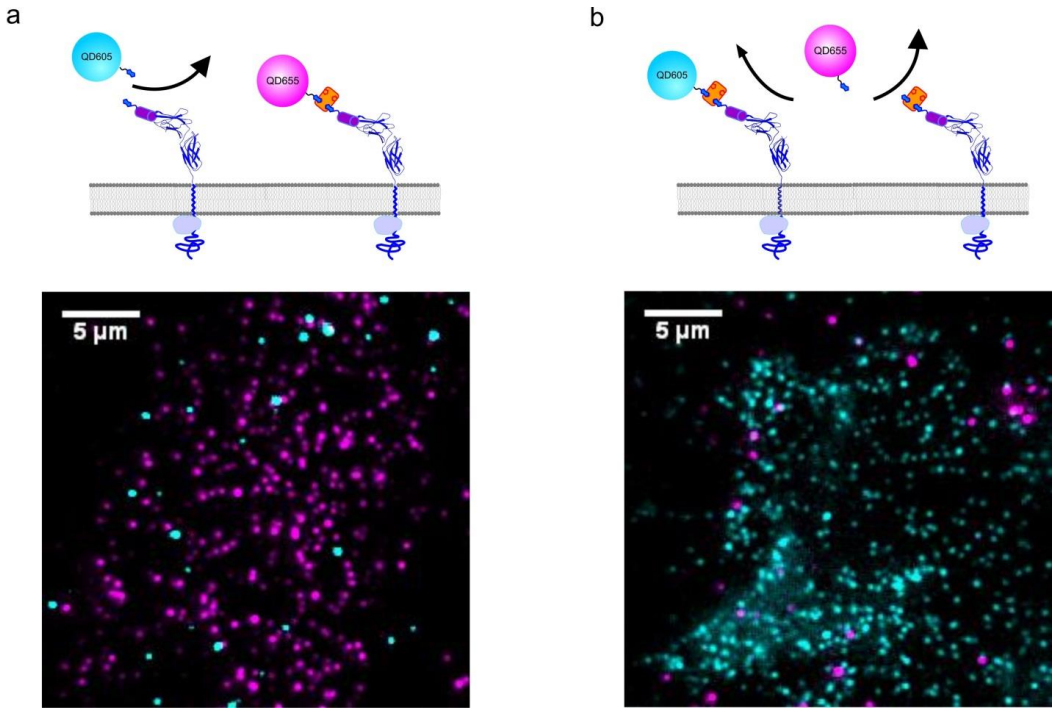

fig. S4. Orthogonal labeling of IFNAR1 and IFNAR2 with monovalent QD. (**a**) QD labeling specificity was shown that the biotinylated SNAP-IFNAR2 cannot be labeled in the absence of bivalent streptavidin (bSAV). (**b**) Confirmation of labeling orthogonality: After SNAP-IFNAR2 was successfully labeled with ^{BT}QD605, by blockage with excess biotin, bSAV-SNAP-IFNAR2 could no longer be labeled by ^{BT}QD655.

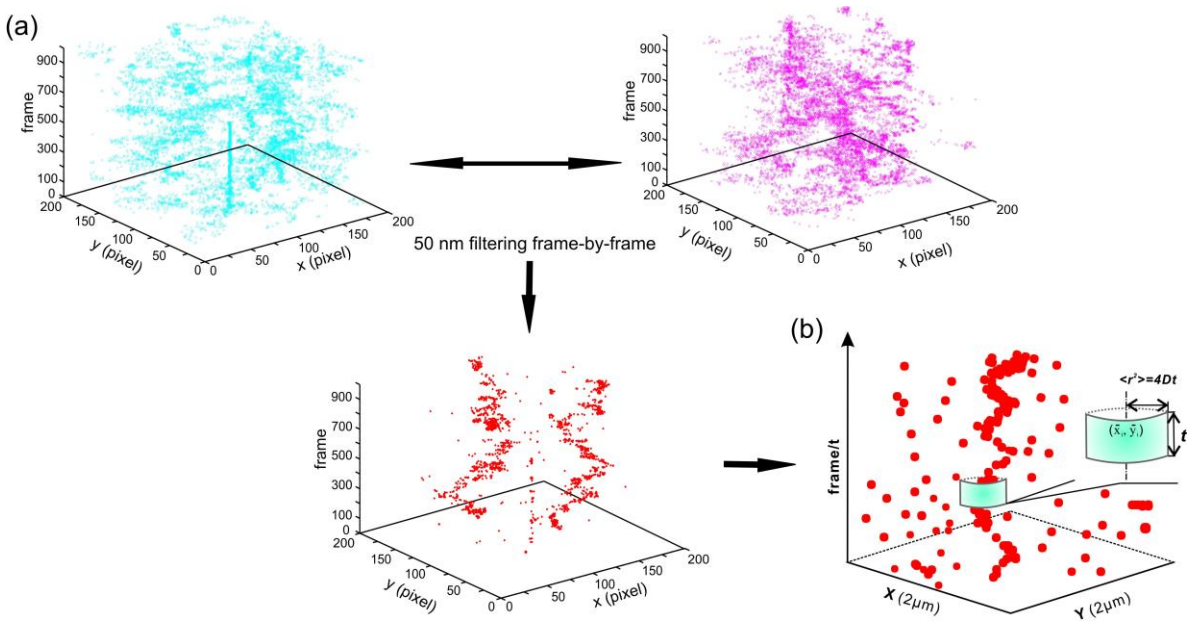

fig. S5. High-fidelity colocomotion analysis. (**a**) Scheme for filtering the colocalized particles using a distance threshold of 50 nm. (**b**) Subsequently, time lapse particle correlation is applied to the filtered dataset for long-term tracking of the colocalized QD-labeled receptors (details are provides in the Supplementary Methods section 1.8).

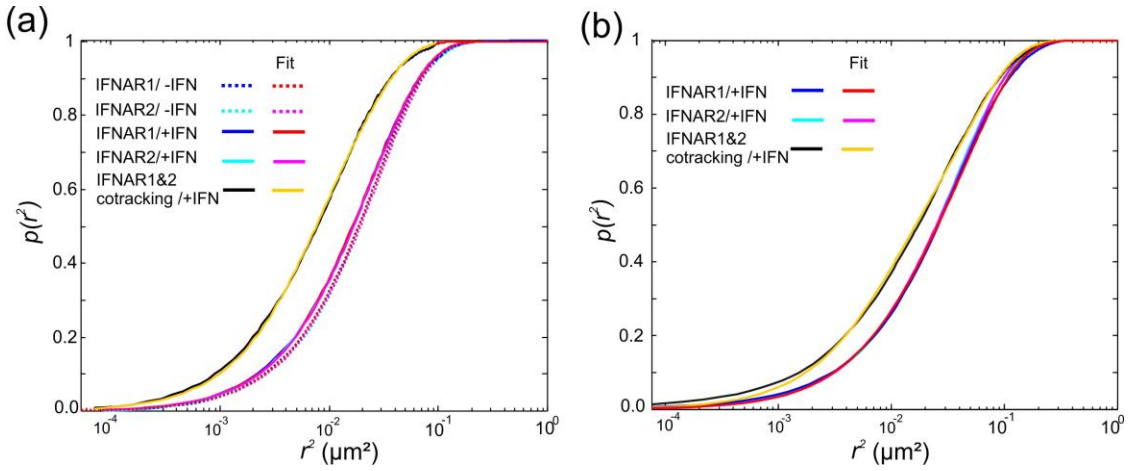

fig. S6. Role of the MSK for receptor diffusion. (**a**) Diffusion properties of IFNAR1 and IFNAR2 in absence and in presence of IFN represented by cumulative probability plots of square displacement for QD-labeled receptors. A two-component equation (Eqn. 1) was used for nonlinear least squares fitting of the curves and for extrapolating the diffusion constants. (**b**) The same curves as in (a) for cells treated with LatB. Each curve was calculated from several thousand trajectories recorded within 2000 frames at an acquisition rate of 32 ms per frame.

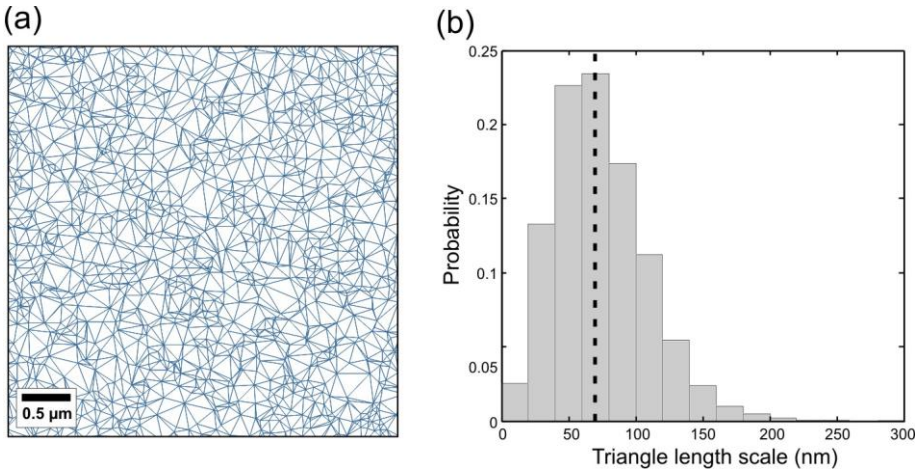

fig. S7. Model of the stochastic MSK meshwork used for simulations. (**a**) 4×4 µm^2 crop of the center of the 10×10 µm^2 MSK-compartmentalized plasma membrane model. (**b**) Compartment size distribution (bin size 20 nm) with a median of ~70 nm (dashed black line).

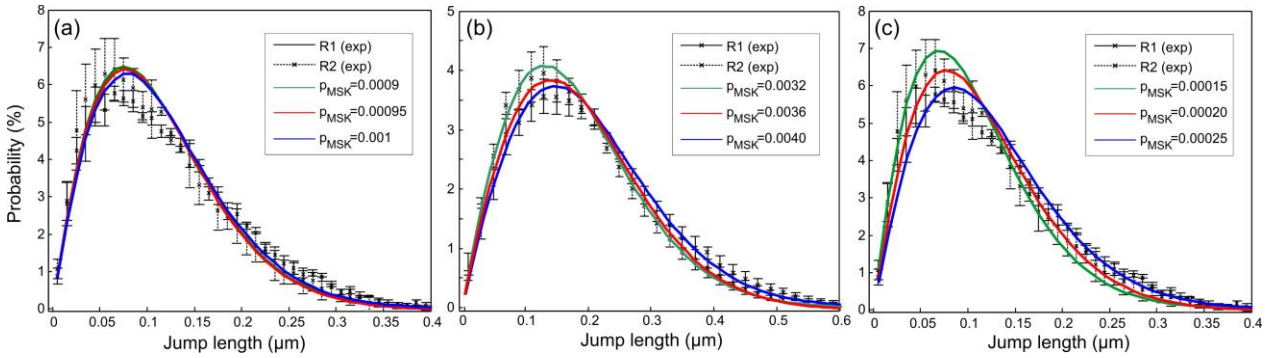

fig. S8. Fitting of hop probabilities of the MSK model. (**a**) Good agreement of simulated curves (green) with experimentally derived 160 ms jump length distributions (160ms-JLDs) for IFNAR1 (dark gray) and IFNAR2 (light gray) was achieved with $p_{\mathrm{MSK}} = 0.00095$ for model parameters $D_{\mathrm{R1/R2}} = 1.1$ µm^2/s and $\Delta t = 0.005$ ms. (**b**) Fitting of 160ms-JLDs of R1 and R2 after LatB treatment for model parameters $D_{\mathrm{R1/R2}} = 1.1$ µm^2/s and $\Delta t = 0.005$ ms. The best fit was obtained with $p_{\mathrm{MSK}} = 0.0036$. (**c**) For model parameters $D_{\mathrm{R1/R2}} = 5$ µm^2/s and $\Delta t = 0.0011$ ms, the best fit (green) of 160ms-JLDs was achieved with $p_{\mathrm{MSK}} = 0.0002$.

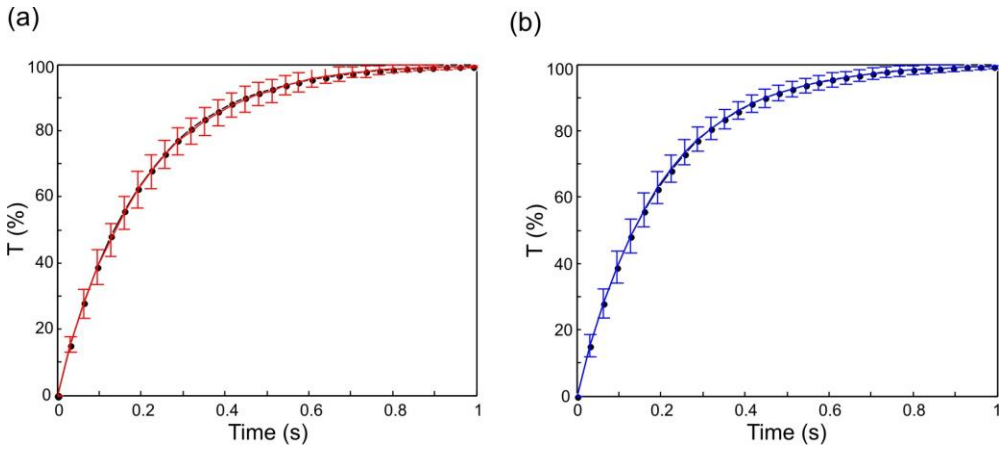

fig. S9. Fitting of association probabilities. Here, fits (solid lines with error bars) of experimentally derived association dynamics (black dots) were achieved for model parameters $D_{\mathrm{R1/R2}} = 1.1\mu\mathrm{m}^2/\mathrm{s}$, $\Delta t = 0.005\mathrm{ms}$ and binding radii (**a**) $r_{\mathrm{on}} = 5\mathrm{nm}$ and (**b**) $r_{\mathrm{on}} = 10\mathrm{nm}$. The corresponding association probabilities are (a) $p_{\mathrm{on}} = 0.0068$ and (b) $p_{\mathrm{on}} = 0.0017$, respectively.

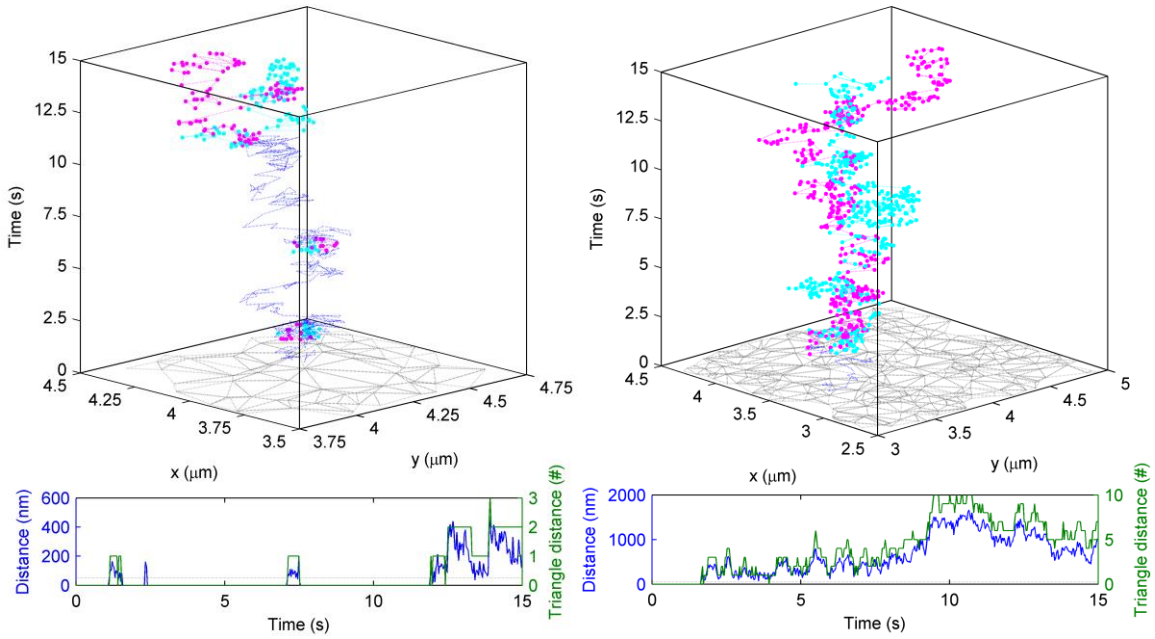

fig. S10. Sample simulations of ternary complex dissociation and reassociation. Representative trajectories in the absence (left) and the presence (right) of LatB, the latter being reflected in the nearly 4-fold increased hop probability. Details of the triangle mesh are indicated at the bottom of the 3D trajectory. IFNAR1, IFNAR2 and the ternary complex are shown in cyan, magenta, and blue, respectively. In addition, individual receptor positions are marked with a dot. The distance in nm between the two receptors (blue) as well as the distance between the triangles that contain the two receptors (green) is shown below. We define triangle distance as the number of point neighbors (triangles that have at least on corner point in common) that the triangles containing IFNAR1 and IFNAR2 are apart. For instance, if the two receptors are in neighboring triangles, then the triangle distance is 1, and if the triangles containing IFNAR1 and IFNAR2 are not direct point neighbors but connected by another triangle, then the triangle distance is 2. In average, receptors separate through hop diffusion significantly faster than those in the untreated scenario. This could be expected from the considerably larger hop probability, under confinement conditions similar to those of LatB treated membranes.

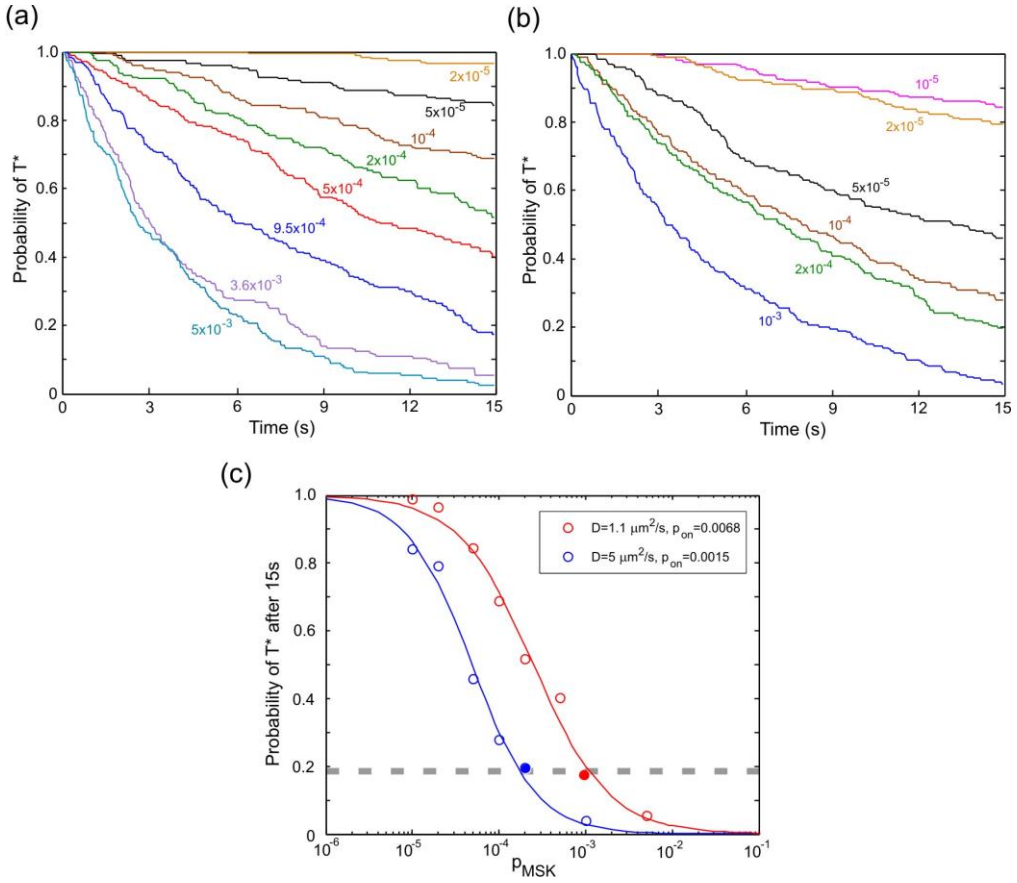

fig. S11. Dependency of simulated receptor complex lifetime on MSK hop probability. (**a**, **b**) Average colocalization probability dynamics over 15 s ($p_{\mathrm{T*@15s}}$) measured according to criterion III. The input diffusion coefficient $D_{\mathrm{R1/R2}}$ is 1.1 μm^2/s for (a) and 5 μm^2/s for (b), respectively. Different colors represent different values of p_{MSK} as indicated in the figure. (**c**) The simulated lifetime is not sensitive to the input diffusion constants in simulations. Comparison of $p_{\mathrm{T*@15s}}$ *vs* p_{MSK} plots for $D_{\mathrm{R1/R2}} = 1.1$ μm^2/s (red) and $D_{\mathrm{R1/R2}} = 5$ μm^2/s (blue). The resulting plots were fitted with a negative sigmoidal function $f(p_{\mathrm{MSK}}) = 1/\left(1 + (a\, p_{\mathrm{MSK}})^b\right)$, where MSK hop probabilities $p_{\mathrm{MSK}} = 0.00095$ for D= 1.1 μm^2/s and $p_{\mathrm{MSK}} = 0.0002$ for D= 5 μm^2/s are marked with solid circles in red and blue, respectively. The dashed line highlights that a similar MSK stabilization effect was obtained by different input diffusion constants.

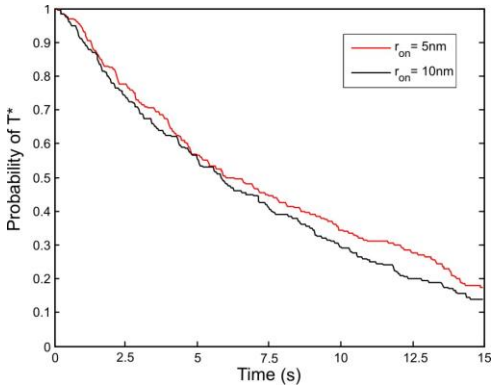

fig. S12. Effect of the reaction radius on the simulated receptor complex lifetime. Comparison of the colocalization probability dynamics for $r_{\mathrm{on}} = 10\mathrm{nm}$, $p_{\mathrm{on}} = 0.0017$ (red) and $r_{\mathrm{on}} = 5\mathrm{nm}$, $p_{\mathrm{on}} = 0.0068$ (black) for the hop probability $p_{\mathrm{MSK}} = 0.00095$.

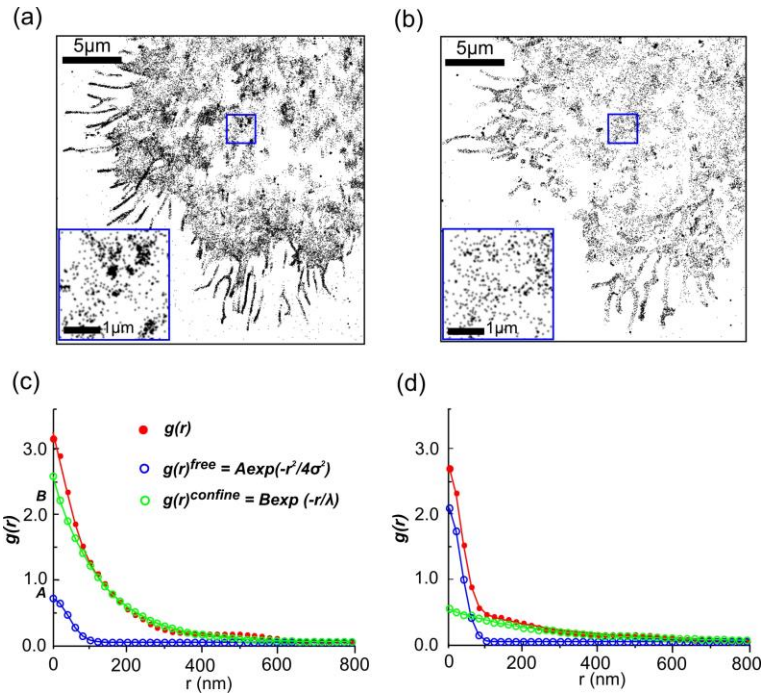

fig. S13. TALM and pcTALM analyses of receptor confinement. (**a**) TALM image of $^{\mathrm{QD}}$IFNAR2 reconstructed from 100 frames in 25.6 s. Inset is a magnified image of the region outlined by the blue square for pair correlation analysis. (**b**) TALM image of the same cell after LatB treatment. (**c**) Pair correlation analysis of inset in (a). The two components in the pair correlation function are shown in blue for $g(r)^{\mathrm{free}}$ and green for $g(r)^{\mathrm{confine}}$ respectively. σ is the average localization precision in the TALM image, λ is the average radius of the confinement zone. A confinement probability cp = 0.79 and a confinement radius λ = 130 nm were obtained by nonlinear least squares fitting of $g(r)$ using Eqn. 3. (**d**) LatB treatment disrupted compartmentalization of IFNAR2 on HeLa cell surface. Pair correlation result for the inset of (b) shows cp =0.18 and λ=354 nm in the same region after LatB treatment.

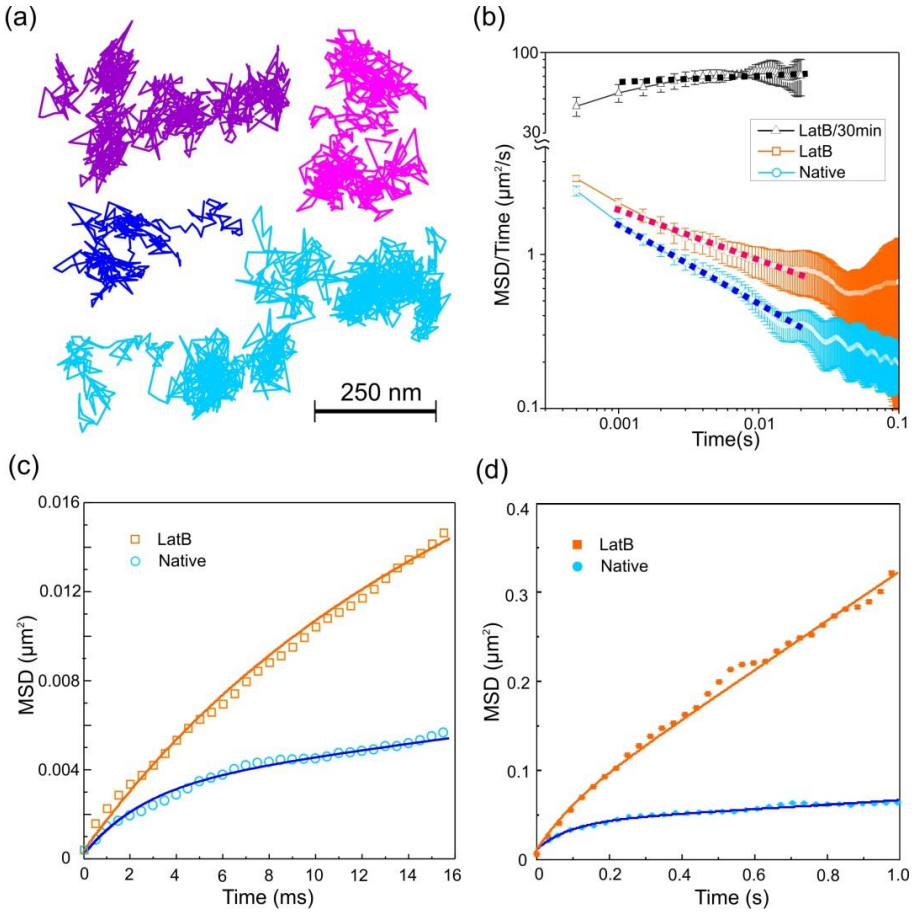

fig. S14. Primary and secondary confinement confirmed by tracking receptors at 2000 Hz. (**a**) Typical trajectories of QD-labeled IFNAR1 recorded at a time resolution of 0.5 ms at the plasma membrane of native cells. (**b**) MSD/time vs. time plot according to Eqn. 5 confirms transient confinement of receptors in the plasma membrane of native cells. LatB treatment changes the anomalous diffusion coefficient α to 0.67 (orange) as compared to 0.54 for untreated cells (blue), thus confirming reduced confinement. Fully Brownian diffusion was only observed in cells that transformed into giant vesicle-like blebs after 30 min LatB treatment (black). (**c**, **d**) Dimensions and residence times of primary and secondary compartments as obtained from MSD analysis. (c) MSD plot at a temporal resolution of 0.5 ms (symbols) and fit of Eqn. 7 (solid lines). Parameters obtained from the fit are summarized in Supplementary table S4. Trajectory numbers for native and LatB-treated cell were 386 and 1737, respectively. (d) MSD curves at a temporal resolution of 32 ms applied to the trajectories of the same experiments to characterize transient confinement by secondary compartments. Fitting according to Eqn. 7. Parameters obtained from the fit are summarized in Supplementary table S4.

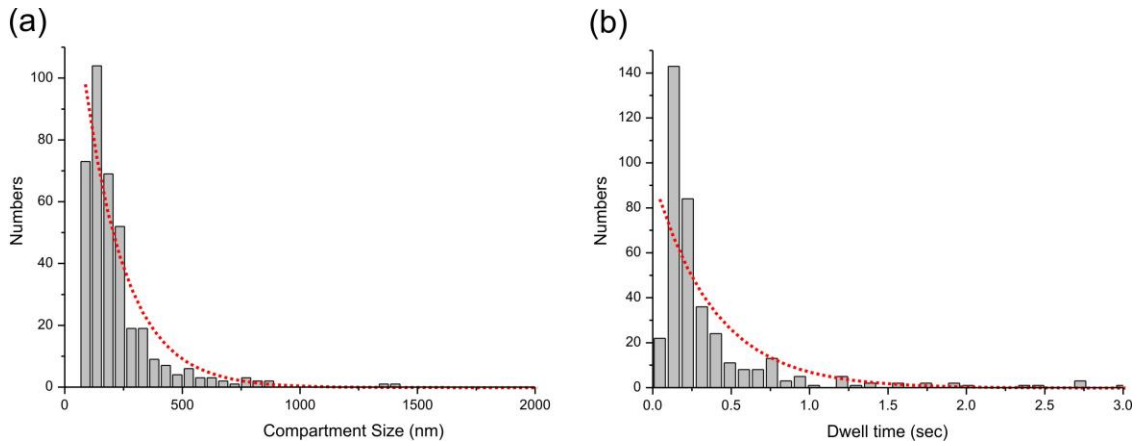

fig. S15. Compartment size and dwell time determined by DBSCAN analysis of fast TALM images. Histograms are based on the analyses of 386 clusters identified from the fast TALM images acquired in 7.5s at 2000 Hz for 24 QD-labeled IFNAR1s. The characteristic value is 270±76 nm for (**a**) and 0.43±0.08 s for (**b**), respectively, according to the mono-exponential fit.

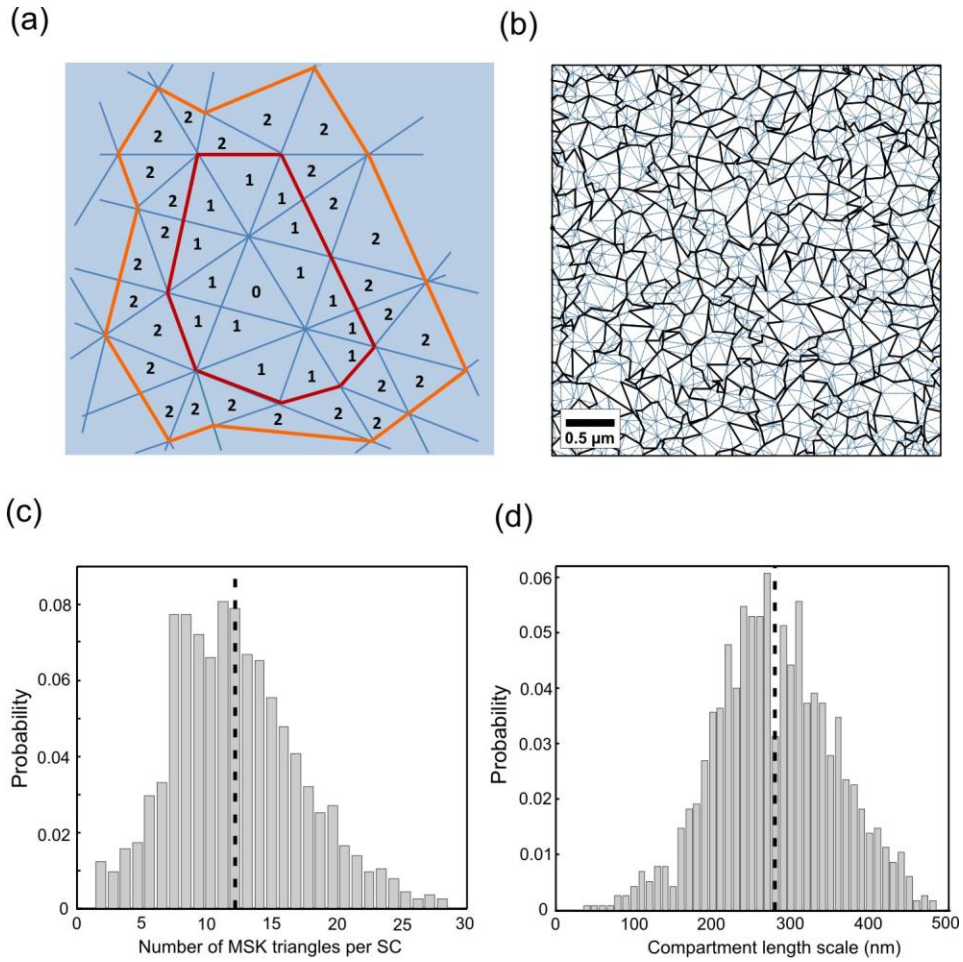

fig. S16. Spatial stochastic model for simulating hierarchical confinement zones. (**a**) Scheme for illustration of the first two steps of the growth algorithm for generating secondary compartments: SC boundaries overlap with MSK triangle sides. Starting from a randomly chosen MSK triangle ('0'), the SC growths by iteratively adding SC-neighboring triangles. In the first round all triangles are marked with '1', and in the second round all triangles are marked with '2'. (**b**) Secondary (solid black lines) and MSK compartmentalization (thin blue lines) of the 4×4 µm^2 crop of the center of the 10×10 µm^2 domain (see figure S7). (**c**) Histogram of SC length scales, i.e. of the square roots of SC areas (median: 279.1 nm). (**d**) Histogram of number of MSK triangles per SC (median: 13 triangles). The median of each distribution is indicated with a dashed line.

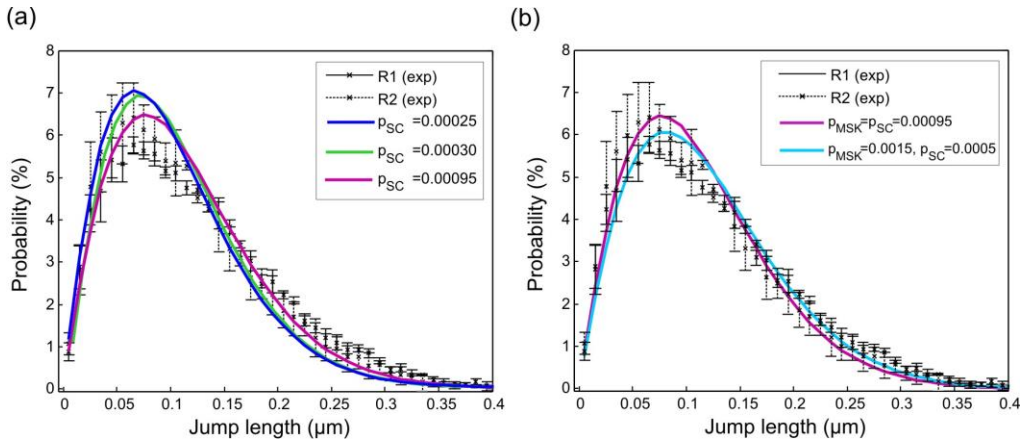

fig. S17. Fitting of hop probabilities in the refined MSK model. (**a**) Fits of experimentally derived 160 ms jump length distributions (160ms-JLDs) for R1 (dark line) and R2 (dash line), for fixed $p_{\mathrm{MSK}} = 0.00095$ and varying p_{SC} (blue, green and purple). $D_{\mathrm{R1/R2}} = 1.1\mu\mathrm{m}^2/\mathrm{s}$ and $\Delta t = 0.005\mathrm{ms}$. (**b**) Fit (cyan) of same 160ms-JLDs when varying both $\mathrm{p_{MSK}}$ and $\mathrm{p_{SC}}$ independently.

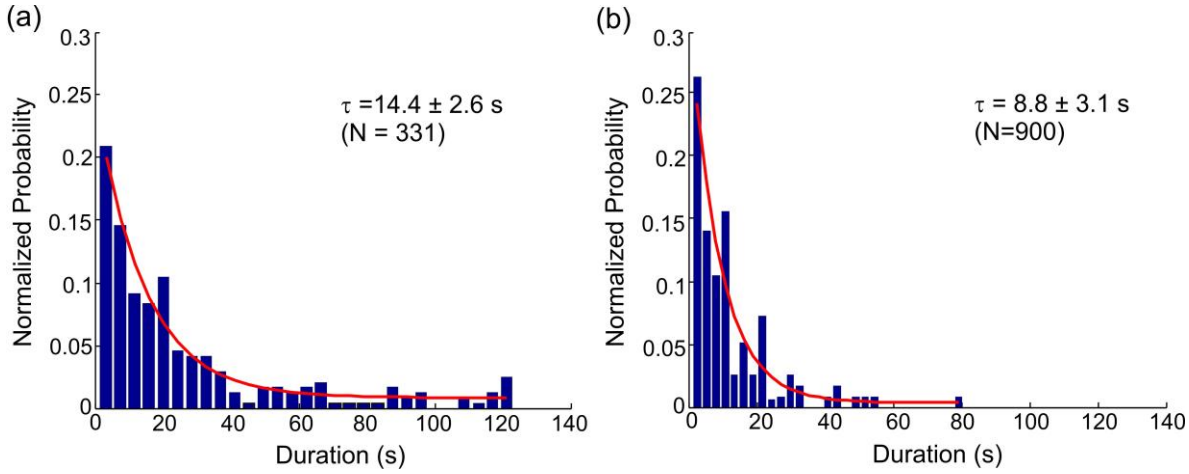

fig. S18. Experimental trajectory length histograms for different colocalization cutoffs. (**a**) Complex lifetime of 14.4±2.6s was determined when transient dissociation events were ignored. The evaluation is based on 331 colocomoting trajectories. (**b**) When transient dissociations were set as the separations of ternary complex, a lifetime of 8.8 ± 3.1 s was obtained. For this evaluation, colocomotion events with the distances between IFNAR1 and IFNAR2 larger than 200 nm are excluded from the same colocomotion data of (a). As a result, the transient dissociation events break the 331 trajectories into 900 shorter ones.

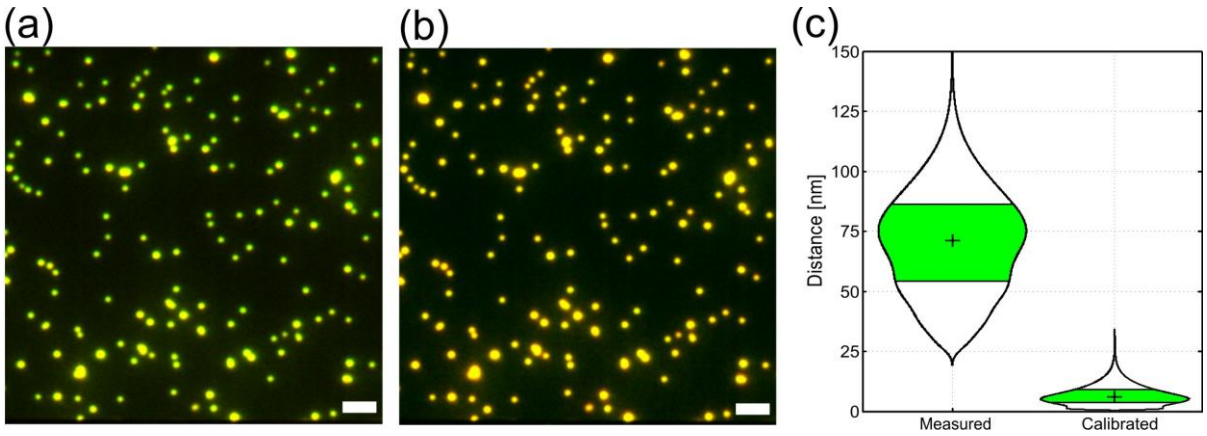

fig. S19. Channel alignment for colocalization analysis. (**a**) Overlay image of multicolor fluorescent TetraSpeck® microspheres visualized in two spectral channels: 585nm/40nm (green) and 670nm/30nm (red). (**b**) Overlay image after correcting the channel alignment by a transformation matrix, which was calculated based on Matlab's function *cp2tform* with type 'affine'. Scale bars: 2µm. (**c**) Assessment of channel deviations before and after alignment correction. Distances between the localized centers of identical emitters detected in each channel were calculated. Average channel deviations of 7.3 ± 4.0 nm (median ± 50%CI) were obtained after alignment, compared to 71 ± 22 nm without correction.

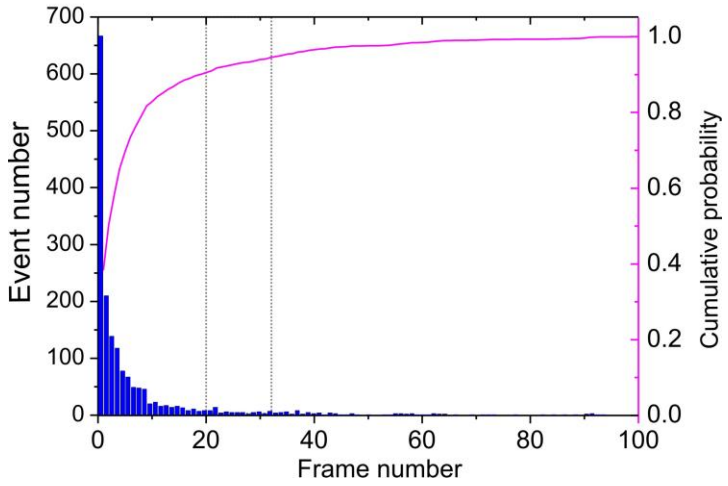

fig. S20. Determination of the observation window for time-lapse pcTALM. QD pairs adsorbed to the coverslide surface were monitored in a time-lapse manner. The number of events associated with simultaneous detection of both QDs against the number of frames between consecutive detections were plotted. Co-blinking frequencies of those immobile QD pairs were assessed based on the recorded frame intervals (magenta curve, right axis). Dashed lines mark the frame numbers where the cumulative probability of observing both QDs is 0.90 and 0.95, respectively.

Supporting Movies

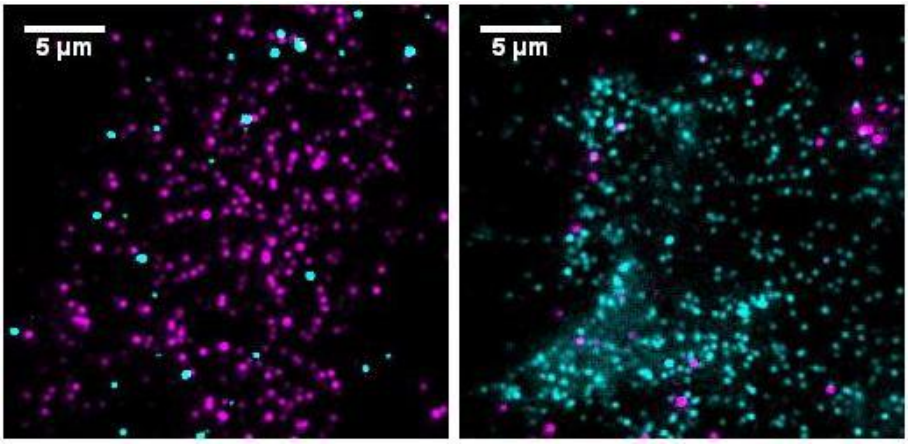

movie S1. Controls confirming the labeling specificity. (Left) Labeling specificity was confirmed by comparison of a few ^{BT}QD605 binding to biotinylated SNAP-IFNAR2 without bSAV, and significant binding of ^{BT}QD655 after bSAV incubation on the same cell. (Right) Orthogonality of stepwise QD labeling. Very few nonspecifically bound ^{BT}QD655 were observed on the cell surface after ^{BT}QD605-labeled SNAP-IFNAR2 was blocked by excess biotin in cell culture medium. Color assignment: QD655 (magenta), QD605 (cyan).

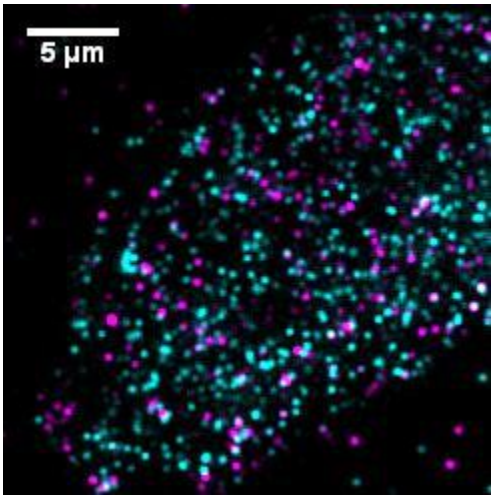

movie S2. Dual-color single-molecule imaging of QD-labeled IFNAR1 and IFNAR2 in a live cell. After successful QD labeling of the two receptors, TIRF images were acquired at 30 frames-per-second in each channel and merged. Movie is played at real time. Color assignment: ^{QD655}IFNAR2 (magenta), ^{QD605}IFNAR1 (cyan).

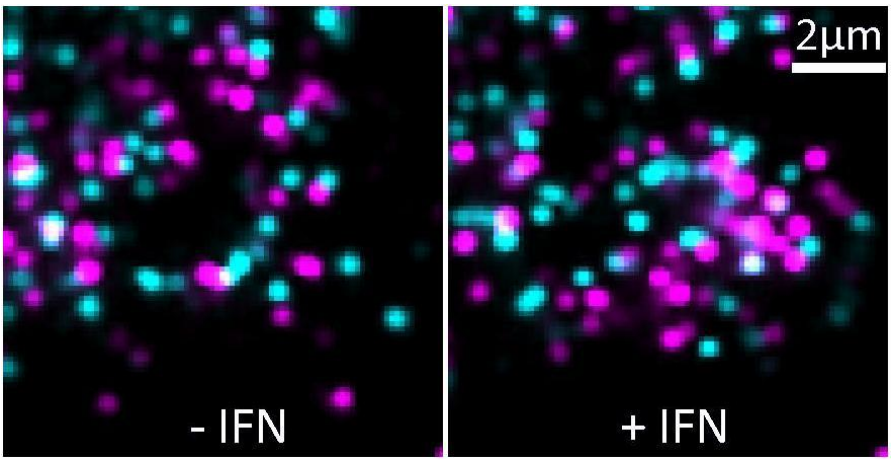

movie S3. Characterization of receptor diffusion before and after IFN stimulation. Real time movie of QD labeled receptors in the same area of the same cell, before and after 2 min of IFN addition. Color assignment: ^{QD655}IFNAR2 (magenta), ^{QD605}IFNAR1 (cyan).

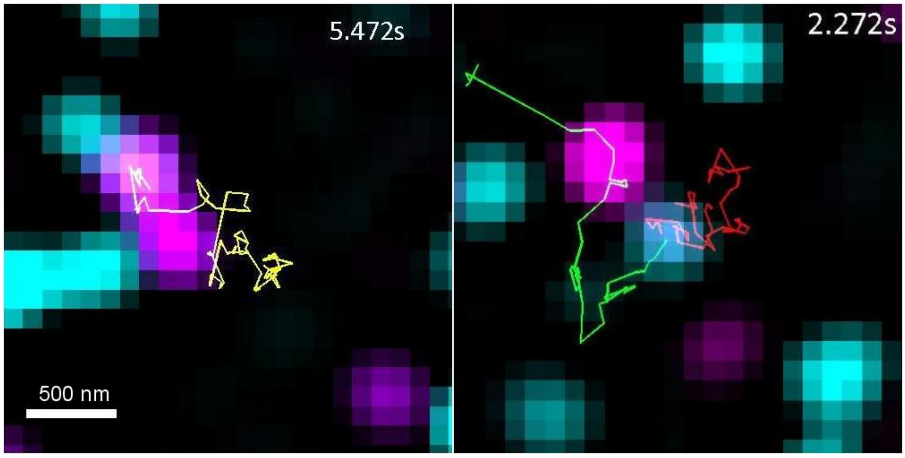

movie S4. Assembly and dissociation of ternary complexes revealed by single-molecule tracking. Left: Dissociation of receptor hetero-dimer. Right: Formation of receptors heterodimer. ^{QD655}IFNAR2 (magenta, trajectory shown in red), ^{QD605}IFNAR1 (cyan, trajectory shown in green), colocomotion trajectory (yellow).

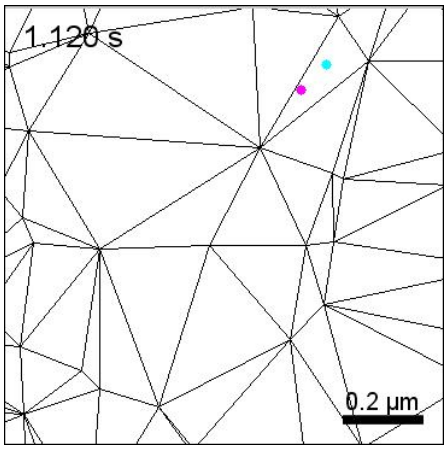

movie S5. Diffusion, dissociation, and reassociation of an individual ternary complex in the MSK meshwork, as obtained from spatial simulations.

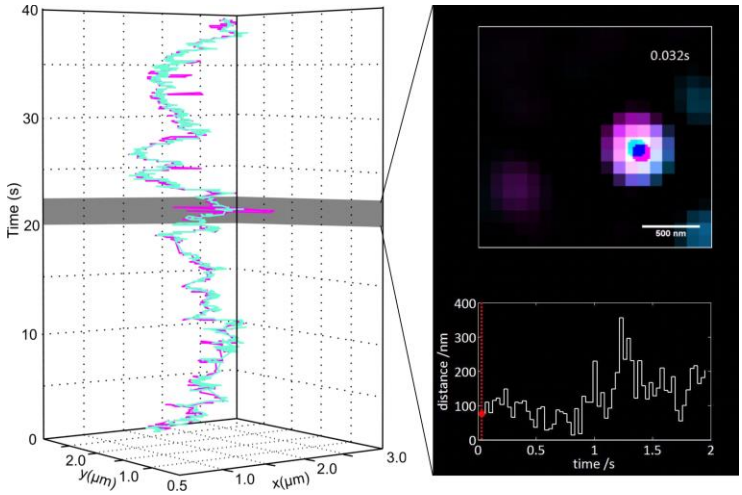

movie S6. Experimentally observed receptor rebinding events. Left: A 3D trajectory of co-locomoted ^{QD655}IFNAR2 (magenta) and ^{QD605}IFNAR1 (cyan). Images were acquired at 30 Hz in each channel and merged. Gray area highlights the time window shown in the movie. Right: The localization centers of receptor-bound QDs were Gaussian blurred with an average localization precision of 20 nm.

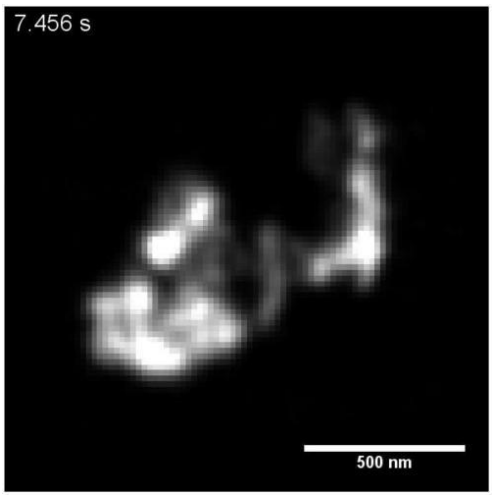

movie S7. Transient receptor confinement at the native cell PM observed by fast TALM. The raw TIRF image was acquired at 2000 Hz for IFNAR1 labeled by QD655. To demonstrate the dynamic transient confinement zone, TALM images within an observation window of 20 ms (40 frames) were reconstructed. Movie playback is ½× real time.